11. F. Verbunt, in *Omega Centauri, A Unique Window into Astrophysics*, F. van Leeuwen, J. D. Hughes, F. Piotto, Eds. (ASP Conference Series no. 265, ASP, San Francisco, CA, 2002), p. 289.
12. C. O. Heinke *et al.*, *Astrophys. J.* **590**, 809 (2003).
13. D. Pooley *et al.*, *Astrophys. J.* **591**, L131 (2003).
14. S. Sigurdsson, E. S. Phinney, *Astrophys. J. Suppl. Ser.* **99**, 609 (1995).
15. S. R. Kulkarni, S. B. Anderson, in *Dynamical Evolution of Star Clusters–Confrontation of Theory and Observations*, P. Hut, J. Makino, Eds. (International Astronomical Union Symposium no. 174, Kluwer, Dordrecht, Netherlands, 1996), p. 181.
16. H. N. Cohn, P. M. Lugger, J. E. Grindlay, P. D. Edmonds, *Astrophys. J.* **571**, 818 (2002).
17. A. S. Fruchter, W. M. Goss, *Astrophys. J.* **536**, 865 (2000).
18. The 442-ms pulsar J1748−2444 was initially identified as Ter 5 B (B1744−24B) but is now known to be a foreground pulsar unrelated to Terzan 5 (*20*).
19. A. G. Lyne *et al.*, *Nature* **347**, 650 (1990).
20. A. G. Lyne, S. H. Mankelow, J. F. Bell, R. N. Manchester, *Mon. Not. R. Astron. Soc.* **316**, 491 (2000).
21. S. M. Ransom, thesis, Harvard University, Cambridge, MA (2001).
22. The National Radio Astronomy Observatory is a facility of the National Science Foundation operated under cooperative agreement by Associated Universities, Incorporated.
23. D. Kaplan *et al.*, in preparation.
24. D. J. Nice, S. E. Thorsett, *Astrophys. J.* **397**, 249 (1992).
25. W. E. Harris, *Astron. J.* **112**, 1487 (1996).
26. These comparisons assume a typical pulsar spectral index of −1.6 (*32*).
27. S. M. Ransom, S. S. Eikenberry, J. Middleditch, *Astron. J.* **124**, 1788 (2002).
28. S. M. Ransom *et al.*, *Astrophys. J.* **604**, 328 (2004).
29. Ter 5 E is a candidate (i.e., unconfirmed) pulsar in (*21*).
30. A. G. Lyne *et al.*, *Mon. Not. R. Astron. Soc.* **295**, 743 (1998).
31. E. S. Phinney, S. R. Kulkarni, *Annu. Rev. Astron. Astrophys.* **32**, 591 (1994).
32. D. R. Lorimer, J. A. Yates, A. G. Lyne, D. M. Gould, *Mon. Not. R. Astron. Soc.* **273**, 411 (1995).
33. J. Navarro, G. de Bruyn, D. Frail, S. R. Kulkarni, A. G. Lyne, *Astrophys. J.* **455**, L55 (1995).
34. A. G. Lyne, R. N. Manchester, J. H. Taylor, *Mon. Not. R. Astron. Soc.* **213**, 613 (1985).
35. $S_{1950,min}$ is about 8 μJy for $P \sim$ 2- to 4-ms isolated or long orbital period MSPs.
36. F. A. Rasio, D. C. Heggie, *Astrophys. J.* **445**, L133 (1995).
37. A. S. Fruchter, D. R. Stinebring, J. H. Taylor, *Nature* **333**, 237 (1988).
38. A. R. King, M. B. Davies, M. E. Beer, *Mon. Not. R. Astron. Soc.* **345**, 678 (2003).
39. A. Possenti *et al.*, in *Binary Radio Pulsars*, F. Rasio, I. Stairs, Eds. (ASP Conference Series no. 328, ASP, San Francisco, CA, 2005), p. 189.
40. J. Tassoul, *Astrophys. J.* **444**, 338 (1995).
41. F. A. Rasio, S. A. Shapiro, *Astrophys. J.* **377**, 559 (1991).
42. L. L. Smarr, R. Blandford, *Astrophys. J.* **207**, 574 (1976).
43. N. Wex, *Mon. Not. R. Astron. Soc.* **298**, 997 (1998).
44. E. M. Splaver *et al.*, *Astrophys. J.* **581**, 509 (2002).
45. D. J. Nice, E. M. Splaver, I. H. Stairs, in *Binary Radio Pulsars*, F. Rasio, I. Stairs, Eds. (ASP Conference Series no. 328, ASP, San Francisco, CA, 2005), p. 371.
46. J. M. Lattimer, M. Prakash, *Science* **304**, 536 (2004).
47. The Tempo program is available online at http://pulsar.princeton.edu/tempo.
48. We thank F. Rasio, S. Sigurdsson, and M. van Kerkwijk for extremely useful discussions and J. Herrnstein, L. Greenhill, D. Manchester, A. Lyne, and N. D'Amico for providing or aiding with the Parkes data from 1998 and 2000. J.W.T.H. is a Natural Sciences and Engineering Research Council of Canada Post-Graduate Scholarship–Doctoral fellow. I.H.S. holds an NSERC University Faculty Award and is supported by a Discovery grant and University of British Columbia start-up funds. F.C. thanks support from NSF. V.M.K. holds a Canada Research Chair and is supported by an NSERC Discovery Grant and Steacie Fellowship Supplement, by the Fonds Québécois de la recherche sur la nature et les technologies and Canadian Institute for Advanced Research, and by a New Opportunities Grant from the Canada Foundation for Innovation. D.L.K. is a Pappalardo Fellow.

# Optical Imaging of Neuronal Populations During Decision-Making

K. L. Briggman,[1] H. D. I. Abarbanel,[2,3] W. B. Kristan Jr.[1]*

We investigated decision-making in the leech nervous system by stimulating identical sensory inputs that sometimes elicit crawling and other times swimming. Neuronal populations were monitored with voltage-sensitive dyes after each stimulus. By quantifying the discrimination time of each neuron, we found single neurons that discriminate before the two behaviors are evident. We used principal component analysis and linear discriminant analysis to find populations of neurons that discriminated earlier than any single neuron. The analysis highlighted the neuron cell 208. Hyperpolarizing cell 208 during a stimulus biases the leech to swim; depolarizing it biases the leech to crawl or to delay swimming.

Understanding the mechanisms of behavioral choice would be a major step in bringing together neuroscience, psychology, and ethology (*1*). Research into decision-making has used several different strategies. One very productive approach is to have a primate make a sensory discrimination between very similar stimuli while the activity of neurons in various parts of the nervous system is recorded (*2*–*8*). A second approach uses choice competition: presenting an animal with two stimuli that produce mutually exclusive behaviors (choices), to see which behavior predominates (*9*). This has led to the notion that behavioral choices are hierarchical. The neuronal mechanism originally proposed to underlie behavioral hierarchies was inhibitory interactions among the neurons responsible for triggering the different behaviors (*10*). Later work has found that neurons capable of eliciting one behavior are often activated during other, sometimes conflicting, behaviors (*11*, *12*). Among other things, this observation suggests that individual decision-making neurons can be multiplexed—they contribute to choosing more than one behavior—and that they trigger behaviors by being active with other combinations of neurons.

We used a third approach to study decision-making: choice variability. We presented a nervous system with identical stimuli that repeatedly produce two different, mutually exclusive behaviors with roughly equal proba-

bilities. This approach allowed us to focus on neurons involved in decision-making that are downstream from neurons used to make sensory discriminations.

We used the isolated central nervous system (CNS) of the medicinal leech. Motor neuron activity patterns characteristic of swimming (*13*) and crawling (*14*) can be elicited from isolated preparations by electrically stimulating peripheral nerves. Such sensory stimulation activates mechanosensory neurons in patterns that mimic touching the leech's skin (*15*). Stimulating the same kinds of mechanosensory neurons in different locations on the leech produces characteristic behaviors like swimming or crawling (*16*, *17*). We follow the terminology proposed by Schall (*18*), referring to the different behavioral outputs as choices and the process leading up to a choice as decision-making.

Previously, recording from neurons intracellularly one at a time, then stimulating them to determine their effect on the initiation of behavior, has successfully uncovered interneurons that activate swimming (*19*, *20*), crawling (*21*), and whole-body shortening (*22*). However, to explore how decisions are made by populations of neurons (*11*), we needed to record from many neurons at once (*23*). We therefore used voltage-sensitive dyes (*24*, *25*) that allowed us to record simultaneously from many neurons in a midbody segmental ganglion at a resolution better than 5 mV (*26*).

**The leech CNS makes behavioral choices.** The isolated leech CNS consists of a nerve cord connecting 21 segmental ganglia plus a head and tail brain (Fig. 1A). This preparation generates motor patterns that are recognizable as behaviors observed in in-

[1]Division of Biological Sciences, [2]Department of Physics, University of California–San Diego, La Jolla, CA 92093–0357, USA. [3]Marine Physical Laboratory, Scripps Institution of Oceanography, La Jolla, CA 92093–0402, USA.

*To whom correspondence should be addressed. E-mail: wkristan@ucsd.edu

tact leeches, including swimming and crawling. We exposed one ganglion between ganglia 7 (G7) and 10 (G10) for voltage-sensitive dye imaging. We also recorded extracellularly from at least two peripheral nerves [dorsal posterior (DP) nerves] using suction electrodes. These electrodes were used to both stimulate and record. A train of electrical pulses to a DP nerve mimics a touch to the body wall in an intact leech (15) and can elicit both swimming and crawling (Fig. 1B). By stimulating DP nerves between G13 and G16, we evoked swimming in about half of the trials (blue) and crawling in the other half (red).

Each trial lasted 60 s, with an intertrial interval of three min. Although the nerve activity was recorded for the entire trial, the ganglion was imaged during only the initial 10 s (Fig. 1B, green bar). We imaged the neurons on the ventral surface of a midbody segmental ganglion (Fig. 1C). In each preparation, we were able to resolve 130 to 150 of the ~160 known neurons (27) on the ventral surface. The fluorescence resonance energy transfer (FRET)–based voltage-sensitive dye we used (24, 25) is very sensitive to small membrane potential fluctuations (Fig. 1D). For comparison, we show the raw data from a swim trial and a crawl trial (Fig. 1, E and F). Almost every neuron was activated immediately after each stimulus. There was a clear difference in the activity of many neurons once the motor pattern was apparent in the nerve recordings, usually after ~4 s. These neurons are presumably central pattern generating (CPG) interneurons or motor neurons that generate the swimming or crawling rhythm. We were more interested in activity differences before this time, between the stimulus and 4 s, when the decision between the two behaviors was made.

**Discrimination by single neurons.** The activity patterns of a subpopulation of single neurons were able to discriminate swimming trials from crawling trials. Of the neurons that responded to the stimulus, we observed four classes of responses: nondiscriminating (ND) cells, early discriminating (ED) cells, late discriminating (LD) cells, and transiently discriminating (TD) cells (Fig. 2A). We quantified the earliest discrimination time of each single cell ($t_{SC}$) by performing a sliding window analysis of variance (ANOVA) for each cell (Fig. 2B).

Neurons were ordered by their earliest discrimination times (Fig. 2C). The number of cells that discriminated at some point in time (ED, LD, or TD cells) ranged between 50 and 75% across experiments. We also performed an ANOVA on the nerve recordings (28) to determine the time ($t_{NERVE}$) at which we could discriminate the behaviors on the basis of motor neuron activity (Fig. 2, C and D, green line). We were most interested in cells that discriminate before $t_{NERVE}$ because

these cells are predictive of the behaviors and are candidate decision-making neurons. A histogram of the earliest $t_{SC}$ for each cell shows that 17 cells (mean ± SD = 19 ± 6 cells; $n$ = 6 preparations) discriminated before $t_{NERVE}$ (Fig. 2D).
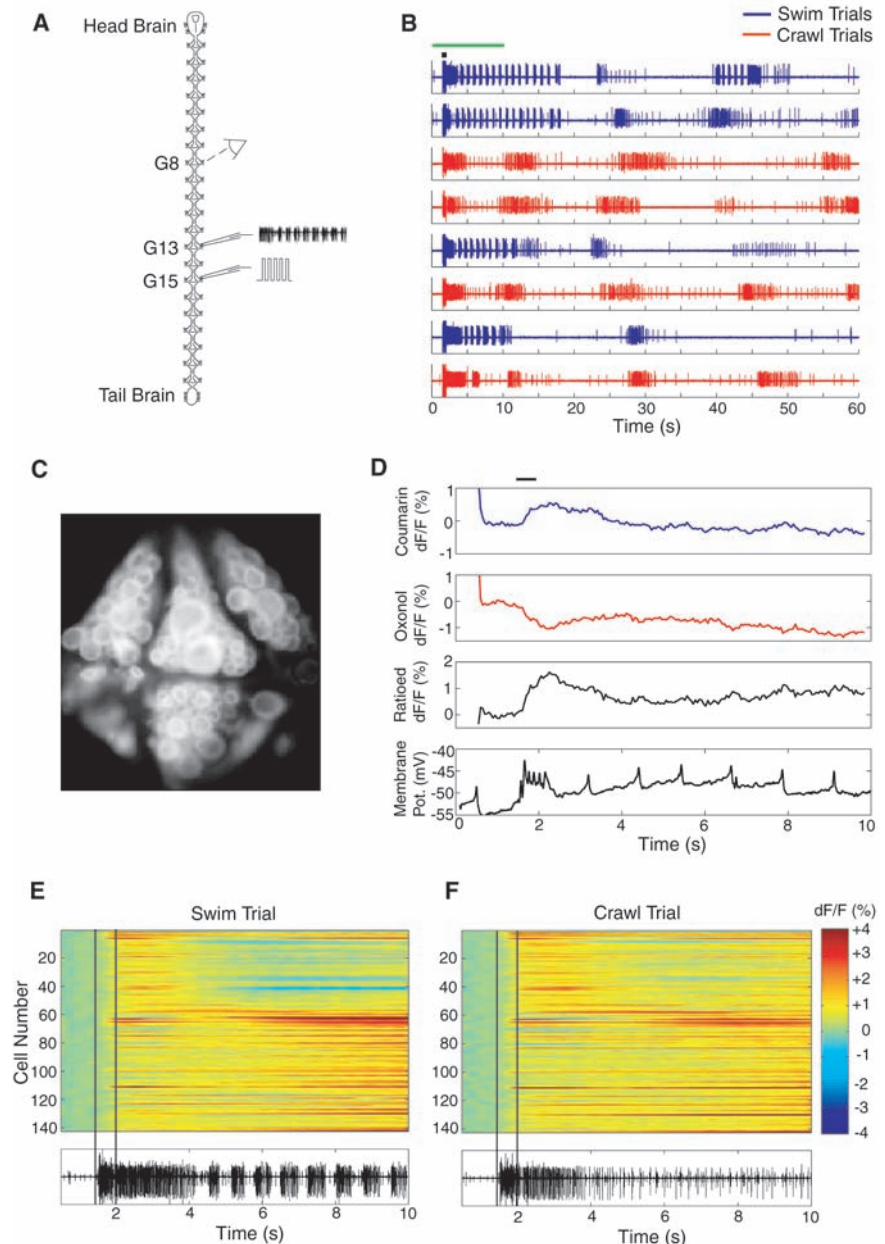


**Fig. 1.** Recording behavioral choices in the isolated leech CNS. (**A**) Schematic of the sites of recording and stimulation. A midbody (G7 to G10) ganglion was imaged with a voltage-sensitive dye. Suction electrodes were used to record from and stimulate DP nerves (DP13 to DP15). (**B**) Eight sequential 60-s trials demonstrated intertrial variability. The stimulus (2 to 3 V, 10-ms pulses at 15 Hz) lasted 300 ms (small black bar). A ganglion was imaged during the initial 10 s of each trial (green bar). Trials are color-coded by behavior: swimming (blue, ~1- to 2-Hz bursts) or crawling (red, ~0.05- to 0.1-Hz bursts). (**C**) The population of neurons (143 in this example) from which we recorded on the ventral surface of a ganglion. (**D**) We averaged the pixels from each neuron to produce a time-varying record of the percentage change in the fluorescence signal (measured as dF/F). The top two traces are the signals from the two dye molecules, coumarin and oxonol. The largest and least noisy signal is the ratio of these two signals (third trace); it was used for all further analysis. The simultaneous intracellular recording (bottom trace) demonstrates the high sensitivity of the dye (15 to 20% per 100 mV). Pot., potential. (**E and F**) Raw optical data from two trials, one which elicited (E) swimming and the other (F) crawling. The optical signal for each neuron is plotted versus time. Color encodes the percent change in fluorescence (dF/F): Positive changes (red) correspond to relative depolarization, and negative changes (blue) correspond to relative hyperpolarization. The panels below each raster plot are simultaneous DP nerve recordings. Vertical black lines indicate the onset and duration of the stimulus.

**Discrimination by populations of neurons.** We view the nervous system of the leech as a dynamical system (*29, 30*). Abstractly, the behavioral state of the nervous system at any instant is a point in the phase space of this system (Fig. 3A). Each axis represents a variable that measures the temporal evolution of trajectories in this space (*31, 32*). For us, these variables are linear combinations of observed neurons. As in the single-cell analysis, we labeled the time at which the trajectories have significantly diverged as the discrimination time. The decision-making period must occur at or before this time. We recognize that the eventual choice may depend on the behavioral state before stimulation, but we did not address this issue in these experiments.

The single-cell discrimination analysis gave us an idea of the number of potential candidate decision-making cells. However, the purpose of simultaneously recording populations of neurons was to look at dynamic interactions among them. Using the multiple recordings, we asked whether a linear combination of neurons could discriminate earlier in time than any single neuron. To address this question, we used two analysis techniques in conjunction: linear discriminant analysis (LDA) (*33*) and principal component analysis (PCA) (*28, 34–36*).

**PCA identifies dimensions that separate behaviors.** For the experiment shown in Fig. 3C, we performed PCA on a data set containing 143 neurons (dimensions) measured across 14 trials. We show the first three principal components (PCs) (Fig. 3B). The bar graphs represent the dimensionless contribution of each neuron to each PC. Values close to zero indicate a small contribution, and high positive or negative values indicate a large contribution. The first three PCs typically account for 60 to 80% of the overall variance in a data set. The remaining 140 PCs are ignored here for visualization purposes. Effectively, we have reduced the dimensionality of the data set from 143 (neurons) to 3 (linear combinations of neurons, the PCs).

We plotted the data three-dimensionally, using the first three PCs as the axes (Fig. 3C). The trajectories all start in one region and then diverge toward two different regions of the space. From this plot, we extract two features: (i) The separation between the trajectories is an objective measure of decision-making. (ii) The neurons that contribute most to this separation (i.e., have large positive or negative values) are most likely to be responsible for making the choice.

Occasionally, we observed a trial such as the one shown in green in Fig. 3C. This trial would have normally been classified as a crawling trial on the basis of the nerve recording. However, the trajectory in the phase space initially diverges in the direction of the swimming trajectories. After a delay, the trajectory turns and moves toward the direction of the crawling trajectories. Although trials such as this were rare (2 out of 60 trials from six experiments), we interpret this as evidence that decision-making is a dynamical process: The leech nervous system can start to make a decision and subsequently change to an alternative choice.

**LDA finds neuronal populations that discriminate.** Having reduced the dimensionality of the data set with PCA, we asked (i) at what time did the swimming and crawling trajectories significantly diverge, and (ii) which neurons are responsible for the separation at this time? We thus divided the temporal trajectories into time bins and estimated the linear discriminant for each bin. We then performed an ANOVA on the data in each respective time bin projected onto each linear discriminant. Therefore, each time bin has an associated *P* value. The time at which this *P* value became significant is denoted $t_{LDA}$. The time bin width and the number of PCs were varied to find the optimal $t_{LDA}$ for each data set (*37*) (fig. S1).

We show an estimated linear discriminant in Fig. 3D using three PCs. Neurons contributing strongly to the linear discriminant were those that best helped discriminate between swimming and crawling at $t_{LDA}$. In this case, PC3 had the largest weighting, so the linear discriminant direction is similar to PC3.

We wished to visualize the spatial locations of the neurons with large-magnitude contributions to the linear discriminant. We
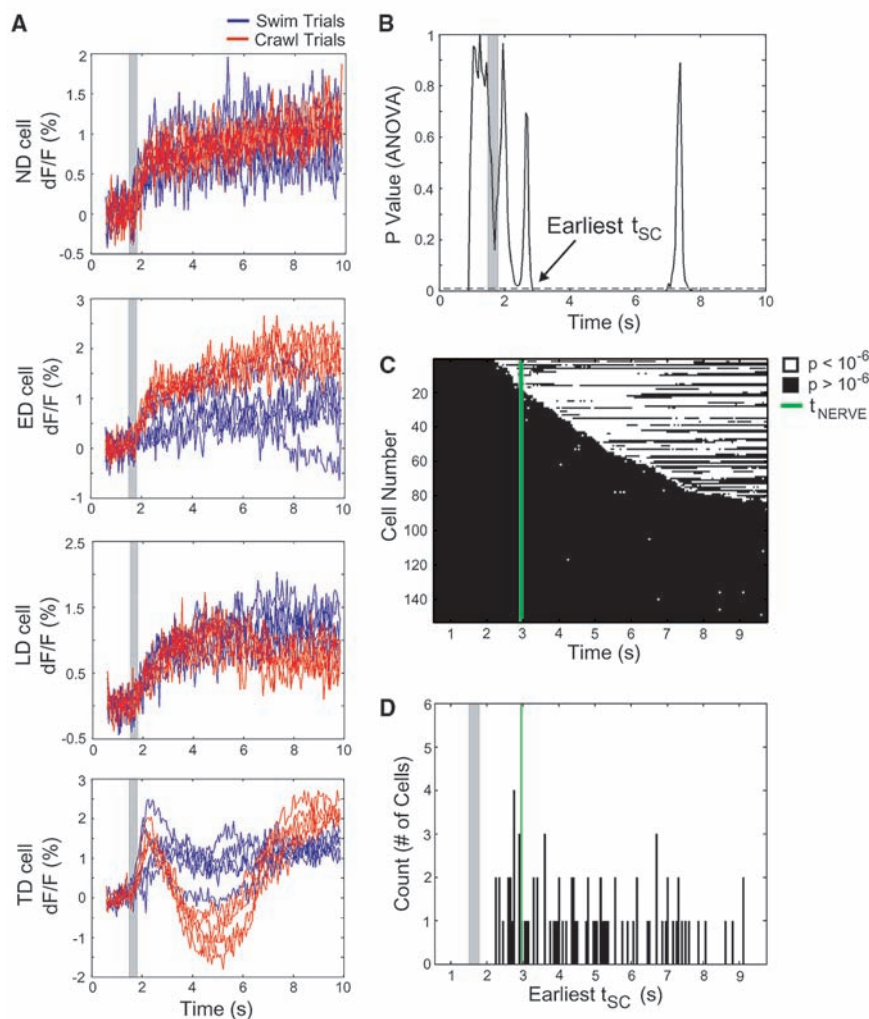


**Fig. 2.** Single-cell discrimination. (**A**) Examples of the four classes of discrimination responses observed. Each graph plots overlapping raw fluorescence traces from five swimming (blue) and five crawling (red) trials for a single cell. In this and all subsequent plots, the gray shaded region denotes the time and duration of the stimulus. (**B**) A sliding-window ANOVA was used to quantify the discrimination times for each cell. The earliest discrimination time ($t_{SC}$) was the time at which the swimming and crawling trajectories significantly diverged (black arrow). (**C**) A raster plot of the ANOVA results from all of the cells from one experiment. Black indicates nonsignificant times, and white indicates significantly different times ($P < 10^{-6}$). The discrimination time based on the nerve recording of the behavior is shown ($t_{NERVE}$, green line). (**D**) A histogram of the earliest $t_{SC}$ from the raster plot in (C). Seventeen neurons produced significantly different trajectories before $t_{NERVE}$.

used color to encode the magnitude of each neuron and projected the colors onto a map of the ganglion (Fig. 3E). This spatial ganglion map was used as a guide for identifying candidate decision-making neurons.

**Discrimination of single neurons versus neuronal populations.** We compared the discrimination times of the earliest single cell ($t_{ESC}$) and the linear discriminant ($t_{LDA}$) from six experiments (Fig. 4A). In all experiments, $t_{LDA}$ occurred before $t_{ESC}$. $t_{SC}$ times (black lines) that occurred before the $t_{NERVE}$ times (green lines) are also plotted.

The neuronal populations contributing highly to the linear discriminant were generally different from the neurons with early single-cell discrimination times (Fig. 4, B and C). Single-cell discrimination times ($t_{SC}$) in Fig. 4C are color-coded, with yellow representing the earliest $t_{SC}$ times and red representing later $t_{SC}$ times. The ganglion maps from all experiments are given in figs. S2 and S3.

**Cell 208 biases decisions.** The analyses described to this point were performed within 15 min during an ongoing experiment, so the ganglion maps were used to identify candidate decision-making neurons. To test whether these neurons were sufficient to influence decision-making individually, we passed polarizing current into each of them during the nerve shock. We impaled each candidate neuron and injected hyperpolarizing or depolarizing current before and after the nerve shock. None of the neurons with early single-cell discrimination times (Fig. 4C) significantly affected the elicited behaviors (33 neurons from six preparations). When we tested neurons contributing strongly to the linear discriminant (17 neurons from six preparations), we found a neuron, cell 208, that can selectively bias the decision to swim or to crawl (Fig. 4B, arrow, and fig. S3). When depolarized or hyperpolarized alone, this neuron did not initiate any behaviors (28). However, when stimulated during a nerve shock, cell 208 biased the decision toward swimming or crawling (Fig. 4D). With cell 208 hyperpolarized, the nerve shock reliably evoked swimming (blue trials); with it depolarized, the nerve shock evoked crawling or delayed swimming (red trials). In five preparations, the correlation between the level of current injection and the observed behavior (Fig. 4E) was significant ($P < 0.01$, Fisher's exact test). We conclude that this neuron plays a role in decision-making. The neuron was labeled with an intracellular dye in all experiments and identified as cell 208 on the basis of its morphology and electrophysiological properties (38).

**Discussion.** One of the central questions we attempted to address is whether decision-making is performed by single neurons or by neuronal populations (39). One extreme proposal is multiple competing circuits in which

decision-making neurons for one behavior act by inhibiting the other behaviors, so that only one behavior occurs at a time (9, 10). At the other extreme would be the complete sharing of decision-making neurons by two or more behaviors, with the dynamics of the network determining which behavior is chosen. In the leech, we hypothesize a middle ground in which decision-making neurons are partially shared, where the dynamics of neuronal populations can determine choices, but individual neurons in these populations can profoundly influence decision-making. This view is supported by our results that (i)
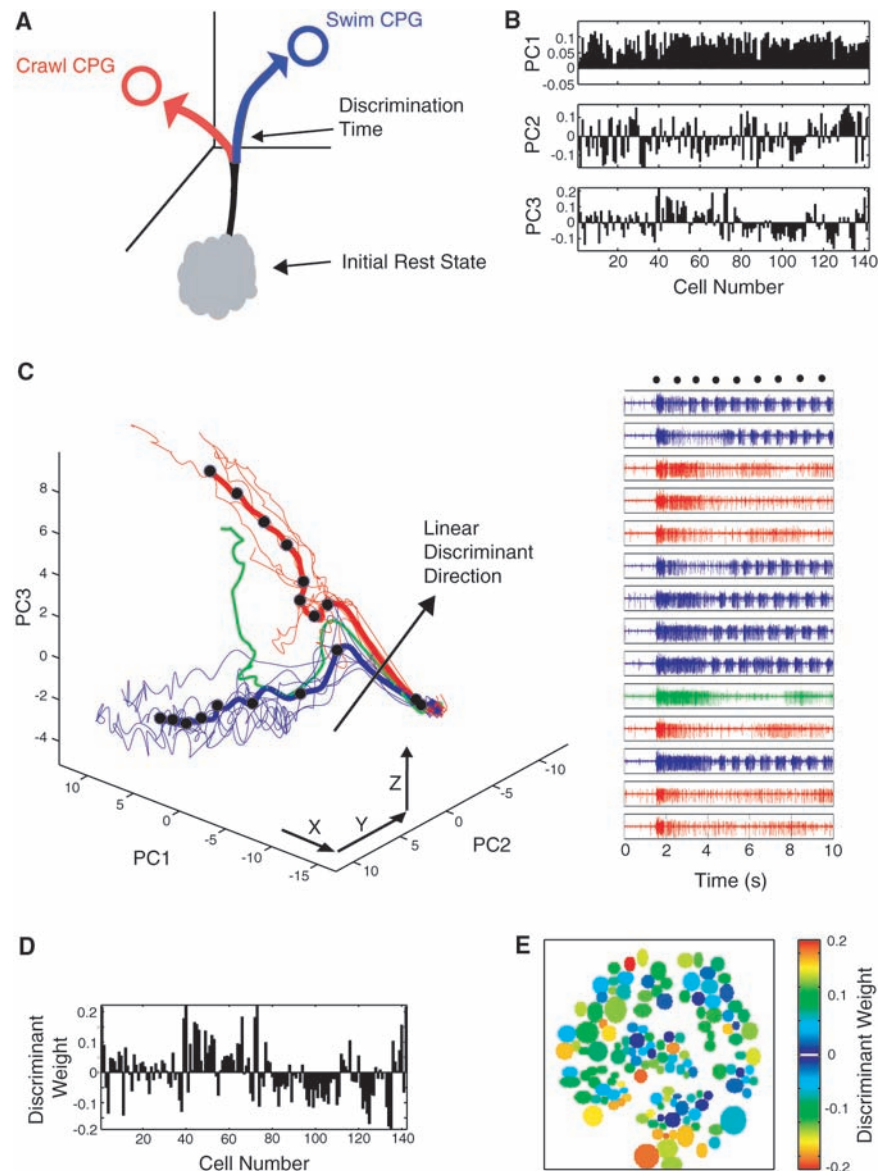


**Fig. 3.** Population discrimination. (**A**) A schematic of our conceptual framework. The state of the leech CNS at any instant is a point in a $d$-dimensional phase space ($d = 3$ in the drawing). The temporal evolution of its state defines a trajectory in this space. Before stimulation, the state of the nervous system is in a rest region. Upon stimulation, the trajectories diverge toward either a swimming or a crawling region on the basis of which choice was made. (**B**) The first PC from a single experiment. Each PC is a linear combination of the observed neurons in the $N$-dimensional data set ($N = 143$ in this experiment). (**C**) The same data as in (B), projected onto the three PC axes. Each trajectory represents a trial (swimming blue, crawling red). The average swimming and crawling trajectories are in bold. Black dots indicate 1-s intervals along the average trajectories. The right panel plots the simultaneous DP nerve recording for each trial. The black arrow illustrates the direction of a linear discriminant estimated for a 500-ms time bin in the PC space. The direction of the linear discriminant is a weighted vector sum of the three PCs with weights $x$, $y$, and $z$. (**D**) The resulting linear discriminant, a linear combination of the three PCs. This direction is similar to that of PC3 in (B). (**E**) The linear discriminant weightings for each of the neurons projected onto a map of the ganglion. Red indicates large-magnitude (both positive and negative) contributions to the linear discriminant direction; blue indicates small contributions.

neuronal populations discriminated between swimming and crawling earlier in time than did single neurons; (ii) none of the single neurons that discriminated early were able to bias the decision; and (iii) although cell 208 was able to bias the decision, it was part of a population defined by the linear discriminant.

The finding that a linear combination of neurons discriminates early in time shows that there is sufficient information in a pop-



**Fig. 4.** Comparing single-cell discrimination to population discrimination. (**A**) The distribution of discrimination times from six experiments. Discrimination times for the LDA ($t_{LDA}$, red), single cells ($t_{SC}$, black), earliest single cells ($t_{ESC}$, cyan), and nerve recordings ($t_{NERVE}$, green) are shown. The average difference between $t_{LDA}$ and $t_{ESC}$ was 290 ± 60 ms (mean ± SEM). Single-cell discrimination times occurring later than the $t_{NERVE}$ for each experiment are omitted. (**B**) The color-coded linear discriminant weightings from a single experiment (color-coding as in Fig. 3E). The black arrow indicates cell 208. (**C**) The color-coded single-cell discrimination times ($t_{SC}$) from the same experiment. Yellow represents the earliest discrimination times, and red represents later discrimination times. (**D**) The result from one experiment. Cell 208 was intracellularly impaled and alternately depolarized (+1.5 nA) or hyperpolarized (−1.5 nA) for the initial 10 s of each trial (black bar). The membrane resistance of cell 208 at rest was ∼50 MΩ. A nerve shock was delivered for 300 ms as in Fig. 1B. In the four trials in which cell 208 was hyperpolarized (blue), the preparation swam within 10 s. In the four remaining trials in which cell 208 was depolarized (red), the preparation either produced the crawling motor pattern or it delayed swimming until the intracellular stimulation ended. (**E**) A contingency table summarizing the pooled results from five preparations. The values in parentheses are the expected counts if the observed behavior did not depend on the stimulus condition.

ulation of neurons for an experimenter to predict the ultimate choice. However, this result demonstrates only that the activity pattern of this network correlates with the eventual choice. To show that this information is used during decision-making, we needed to manipulate the network. Ideally, we would like to selectively hyperpolarize or depolarize a population of individual cells; however, we were technologically limited to stimulating one or two cells at a time.

Although we have not exhaustively tested all candidate neurons detected, most of the neurons tested were not able to bias the behavioral choice. However, we were able to reliably bias the choice with one of the linear discriminant candidates, cell 208. A relatively large depolarization or hyperpolarization of cell 208 biased the choice toward crawling or swimming, respectively. Although this result was statistically significant, cell 208 did not determine the choice on all trials. This less-than-perfect control by cell 208 can probably be credited to the cell 208 homologs in each of the 20 other ganglia (38) that we did not stimulate.

Cell 208 has previously been described as a CPG neuron (38), but a unique one that connects the swim-initiating network to the swim CPG circuit. It has not been shown to trigger behaviors in intact isolated nerve cords. Our results suggest that it is also part of a decision-making circuit, although we do not yet know its role in this circuit or the mechanism by which it biases the system. Although it is possible that cell 208 is driven by a higher-order decision-making neuron, we have shown that it alone is capable of biasing the entire system.

Most recent research about decision-making has focused on value-based choices in which there is always a right and wrong answer (2–8). We propose that the term decision-making should refer to a spectrum of goal-driven behaviors. At the most complex level are conscious, introspective choices that incorporate expected reward (1). At the simplest level are reproducible, predictable reflexes. There is a large area of involuntary, subconscious decision-making that has been neglected. For example, suppose your goal is to walk down the street. Which foot do you lead with? This is a choice that is made without conscious effort and will vary from time to time. Although this choice is goal-directed, there is no correct or incorrect choice. In our reduced preparation, there is no obvious value associated with swimming versus crawling, although both choices would achieve the goal of escaping from a stimulus.

Why then does the leech, a relatively simple nervous system, not respond in a predictable manner? We hypothesize two possibilities: Either the choice depends on the rest state before each stimulus, or the state is reset upon stimulation and then diverges stochastically because of noise in the system. The
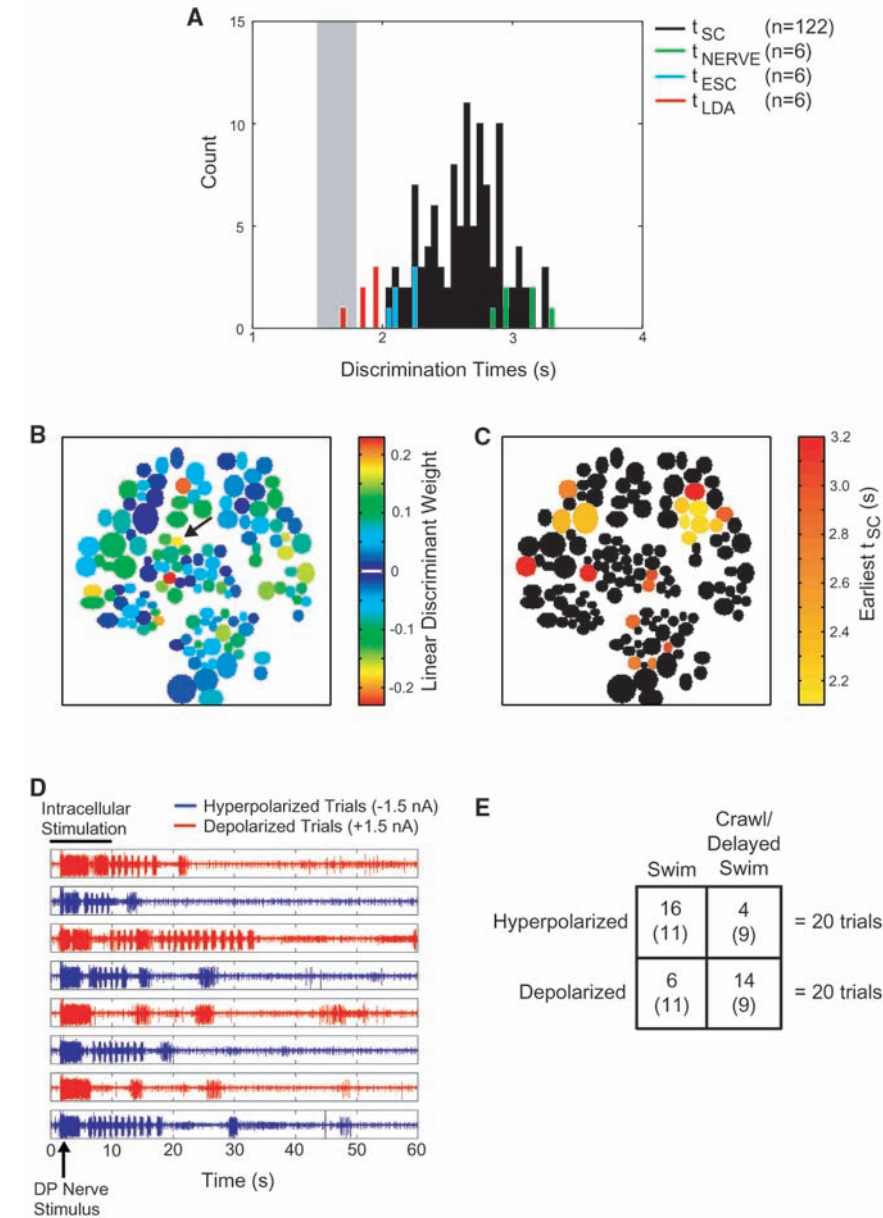
leech may provide a system in which to resolve this important question.

### References and Notes

1. P. W. Glimcher, *Decisions, Uncertainty and the Brain: The Science of Neuroeconomics* (MIT Press, Cambridge, MA, 2003).
2. M. N. Shadlen, W. T. Newsome, *Proc. Natl. Acad. Sci. U.S.A.* **93**, 628 (1996).
3. P. W. Glimcher, *Trends Neurosci.* **24**, 654 (2001).
4. J. D. Schall, *Curr. Biol.* **10**, R404 (2000).
5. M. N. Shadlen, W. T. Newsome, *J. Neurophysiol.* **86**, 1916 (2001).
6. J. I. Gold, M. N. Shadlen, *Nature* **404**, 390 (2000).
7. M. L. Platt, P. W. Glimcher, *Nature* **400**, 233 (1999).
8. R. Romo, E. Salinas, *Annu. Rev. Neurosci.* **24**, 107 (2001).
9. M. P. Kovac, W. J. Davis, *Science* **198**, 632 (1977).
10. M. P. Kovac, W. J. Davis, *J. Neurophysiol.* **43**, 469 (1980).
11. T. Esch, W. B. Kristan Jr., *Integr. Comp. Biol.* **42**, 716 (2002).
12. I. R. Popescu, W. N. Frost, *J. Neurosci.* **22**, 1985 (2002).
13. W. B. Kristan Jr., R. L. Calabrese, *J. Exp. Biol.* **65**, 643 (1976).
14. F. J. Eisenhart, T. W. Cacciatore, W. B. Kristan Jr., *J. Comp. Physiol.* **A186**, 631 (2000).
15. W. B. Kristan Jr., *J. Exp. Biol.* **96**, 161 (1982).
16. W. B. Kristan Jr., S. J. McGirr, G. V. Simpson, *J. Exp. Biol.* **96**, 143 (1982).
17. T. W. Cacciatore, R. Rozenshteyn, W. B. Kristan Jr., *J. Neurosci.* **20**, 1643 (2000).
18. J. D. Schall, *Nature Rev. Neurosci.* **2**, 33 (2001).
19. J. C. Weeks, W. B. Kristan Jr., *J. Exp. Biol.* **77**, 71 (1978).
20. P. D. Brodfuehrer, A. Burns, *Neurobiol. Learn. Mem.* **63**, 192 (1995).
21. T. Esch, K. A. Mesce, W. B. Kristan Jr., *J. Neurosci.* **22**, 11045 (2002).
22. B. K. Shaw, W. B. Kristan Jr., *J. Neurosci.* **17**, 786 (1997).
23. M. Zochowski, L. B. Cohen, G. Fuhrmann, D. Kleinfeld, *J. Neurosci.* **20**, 8485 (2000).
24. J. E. González, K. Oades, Y. Leychkis, A. Harootunian, P. A. Negulescu, *Drug Discov. Today* **4**, 431 (1999).
25. T. W. Cacciatore *et al.*, *Neuron* **23**, 449 (1999).
26. A. L. Taylor, G. W. Cottrell, D. Kleinfeld, W. B. Kristan Jr., *J. Neurosci.* **23**, 11402 (2003).
27. K. J. Muller, J. G. Nicholls, G. S. Stent, *Neurobiology of the Leech* (Cold Spring Harbor, New York, 1981).
28. Materials and methods are available as supporting material on *Science* Online.
29. D. Kaplan, L. Glass, *Understanding Nonlinear Dynamics* (Springer-Verlag, New York, 1995).
30. H. Abarbanel, *Analysis of Observed Chaotic Data* (Springer-Verlag, New York, 1996).
31. D. S. Broomhead, G. P. King, *Phys. D* **20**, 217 (1986).
32. D. S. Broomhead, R. Jones, G. P. King, *J. Phys. A* **20**, 563 (1987).
33. LDA seeks a line in the multidimensional phase space of a system such that grouped data points projected onto the line are maximally separated (i.e., the distributions of swimming versus crawling data points along the line are maximally separated). The slope of this line indicates the relative contribution of each of the variables to this separation. The goal is to find the time at which the swimming and crawling data projected onto a linear discriminant are significantly separated. This technique is susceptible to overfitting when applied in a high-dimensional space with a limited amount of data. To overcome this problem, one may either increase the number of samples or decrease the dimensionality of the system. Phototoxicity limits the amount of data we can collect, so we instead used PCA to reduce the dimensionality of our data sets.
34. PCA rotates the axes of our *N*-dimensional data (where *N* is the number of neurons) so that the first few axes point in the directions of maximal covariance. These new directions are the PCs. A neuron with very different activity between swimming and crawling trials will have a large variance across trials. This neuron would then contribute strongly to one of the first few PCs.
35. R. O. Duda, P. E. Hart, D. G. Stork, *Pattern Classification* (Wiley, New York, ed. 2, 2000).
36. K. Mardia, J. Kent, J. Bibby, *Multivariate Analysis* (Academic Press, San Diego, CA, 1980).
37. The combination of PCA and LDA found linear combinations of neurons that could discriminate the behaviors earlier than any single neuron. Although each of the PCs we discarded did not explain much of the total variance, it is possible that we lost discrimination information by not using them. Thus, although the linear discriminants we found performed well (i.e., discriminated at an early $t_{LDA}$), an earlier $t_{LDA}$ may have been found had we been able to use all of the PCs. This illustrates the inherent tradeoff between the dimensionality of a system and the amount of data required to adequately sample a high-dimensional space.
38. J. Weeks, *J. Comp. Physiol.* **148**, 265 (1982).
39. W. B. Kristan Jr., B. K. Shaw, *Curr. Opin. Neurobiol.* **7**, 826 (1997).
40. We thank J. E. Gonzalez and R. Y. Tsien for assistance with the FRET voltage-sensitive dyes; Panvera LLC for supplying the dyes gratis; C. Schaffer for assistance with designing the wavelength-switching device; J. Shlens, A. L. Taylor, S. B. Mehta, and E. Thomson for valuable discussions; and H. J. Chiel, M. B. Feller, D. Kleinfeld, and T. J. Sejnowksi for helpful comments and suggestions on an earlier version of this manuscript. Supported by a La Jolla Interfaces in Science Predoctoral Fellowship, funded by the Burroughs Wellcome Fund (K.L.B.); a NSF Integrative Graduate Education and Research Traineeship (IGERT) training grant (K.L.B.); NIH research grants nos. MH43396 (W.B.K.) and NS40110 (H.D.I.A); U.S. Department of Energy grant no. DE-FG03-90ER14138 (H.D.I.A); NSF research grant no. PHY0097134 (H.D.I.A); and the Office of Naval Research, contract no. N00014-00-1-0181 (H.D.I.A).

# REPORTS

# Nodal Quasiparticles and Antinodal Charge Ordering in Ca2−xNaxCuO2Cl2

Kyle M. Shen,[1] F. Ronning,[1]* D. H. Lu,[1] F. Baumberger,[1] N. J. C. Ingle,[1] W. S. Lee,[1] W. Meevasana,[1] Y. Kohsaka,[2] M. Azuma,[3] M. Takano,[3] H. Takagi,[2,4] Z.-X. Shen[1]†

Understanding the role of competing states in the cuprates is essential for developing a theory for high-temperature superconductivity. We report angle-resolved photoemission spectroscopy experiments which probe the $4a_0 \times 4a_0$ charge-ordered state discovered by scanning tunneling microscopy in the lightly doped cuprate superconductor Ca2−xNaxCuO2Cl2. Our measurements reveal a marked dichotomy between the real- and momentum-space probes, for which charge ordering is emphasized in the tunneling measurements and photoemission is most sensitive to excitations near the node of the *d*-wave superconducting gap. These results emphasize the importance of momentum anisotropy in determining the complex electronic properties of the cuprates and places strong constraints on theoretical models of the charge-ordered state.

To explain the mechanism of high-temperature superconductivity, it is necessary to understand how the parent Mott insulator, characterized by very strong electron-electron repulsion, can evolve into a high–transition temperature ($T_c$) superconductor upon the addition of a relatively small number of carriers. In the intervening region between the Mott insulator and high-$T_c$ superconductor, the so-called "pseudogap" regime, highly anomalous physical properties have been observed (*1*). Many attempts to explain these unusual properties have centered around the possibility of competing orders, such as orbital currents (*2*), nanoscale charge ordering (*3, 4*), or electronic phase separation (*5*). The particular importance of charge ordering has recently been underscored by the discovery of a distinct real-space pattern of $4a_0 \times 4a_0$ two-dimensional charge ordering (2DCO) in Ca2−xNaxCuO2Cl2 (Na-CCOC) by scanning tunneling microscopy (STM) (*6*). Angle-resolved photoemission spectroscopy (ARPES) can provide crucial

[1]Departments of Applied Physics, Physics, and Stanford Synchrotron Laboratory, Stanford University, Stanford, CA 94305, USA. [2]Department of Advanced Materials Science, University of Tokyo, Kashiwa, Chiba 277–8561, Japan. [3]Institute for Chemical Research, Kyoto University, Uji, Kyoto 611–0011, Japan. [4]RIKEN, The Institute for Physical and Chemical Research, Wako 351–0198, Japan.

*Present address: Los Alamos National Laboratory, Los Alamos, NM 87545, USA.
†To whom correspondence should be addressed. E-mail: zxshen@stanford.edu

# Science

## Optical Imaging of Neuronal Populations During Decision-Making

K. L. Briggman, H. D. I. Abarbanel and W. B. Kristan Jr.

| | |
|---|---|
| **ARTICLE TOOLS** | http://science.sciencemag.org/content/307/5711/896 |
| **SUPPLEMENTARY MATERIALS** | http://science.sciencemag.org/content/suppl/2005/02/10/307.5711.896.DC1 |
| **REFERENCES** | This article cites 29 articles, 12 of which you can access for free http://science.sciencemag.org/content/307/5711/896#BIBL |
| **PERMISSIONS** | http://www.sciencemag.org/help/reprints-and-permissions |

Use of this article is subject to the Terms of Service